

## Measurement of the ionization of slow silicon nuclei in silicon for the calibration of a silicon dark-matter detector

G. Gerbier, E. Lesquoy, J. Rich, M. Spiro, C. Tao, D. Yvon, and S. Zylberajch  
*Centre d'Etudes Nucléaires de Saclay, Département de Physique des Particules Élémentaires,  
 91191 Gif-sur-Yvette CEDEX, France*

P. Delbourgo, G. Haouat, and C. Humeau  
*Centre d'Etudes Nucléaires de Bruyères, DPN/EE, Boîte Postale 12,  
 91680 Bruyères le Chatel, France*

F. Goulding, D. Landis, N. Madden, A. Smith, and J. Walton  
*Lawrence Berkeley Laboratory, Berkeley, California 94720*

D. O. Caldwell, B. Magnusson, and M. Witherell  
*University of California at Santa Barbara, Santa Barbara, California 93106*

B. Sadoulet and A. Da Silva  
*University of California at Berkeley, Berkeley, California 94720*  
 (Received 13 August 1990)

We have measured the ionization produced in a Si(Li) detector by silicon nuclei of kinetic energies in the range 3.2–21 keV. The results are in rather good agreement with the calculations of Lindhard, Scharff, and Schiott and demonstrate the interest of Si(Li) detectors for dark-matter searches. We have also measured the intrinsic fluctuations in the ionization energy due to nucleon recoils.

As first suggested by Goodman and Witten,<sup>1</sup> dark-matter particles in our Galaxy may be detectable via their elastic collisions with nuclei in appropriate detectors. Since nuclei recoil from such collisions with energies in the keV range, the most appropriate existing detectors are germanium and silicon semiconductor detectors. Ultrapure germanium detectors have already placed limits on the masses and cross sections of such particles,<sup>2</sup> ruling out, for instance, Dirac neutrinos of masses greater than 10 GeV as the dominant component of our Galaxy. Because of the lower mass of their constituent nuclei, silicon semiconductor detectors have the capability of extending these limits to lower-mass particles.<sup>3</sup> This is essential for the detection of particles that solve the solar-neutrino problem,<sup>4</sup> the so-called cosmions, which are constrained to have masses in the range 2–12 GeV/c<sup>2</sup>. Results of such an experiment have recently been published.<sup>5</sup>

Since slow recoiling nuclei are expected to produce less ionization than a Compton or photoelectron of the same energy,<sup>6</sup> these detectors must be calibrated. This was done in the 1960s by Chasman<sup>7</sup> for germanium and Sattler<sup>8</sup> for silicon through neutron-nucleus scattering. The measurements on silicon did not extend down to the recoil energies necessary for dark-matter searches. To remedy this situation we have performed an experiment where we have observed silicon recoils in the range 3.2–21 keV.

The experiment was performed at the 4-MeV Van de Graaff accelerator of the Centre d'Etudes Nucléaires de

Bruyères-le-Chatel. The accelerator produces proton pulses of duration about 2 ns every 1  $\mu$ s. The time-averaged current was typically 2  $\mu$ A. The spread in proton energies during the pulse was 12 keV [full width at half maximum (FWHM)] for mean energies near 2 MeV.

Neutrons were produced via the reaction  ${}^7\text{Li}(p,n){}^7\text{Be}$  (threshold = 1.880 MeV). The target consisted of natural lithium evaporated on a tantalum support (which also served as a proton beam stop). For a target thickness of 110  $\mu\text{g}/\text{cm}^2$ , the neutron flux in the forward direction was about  $2.5 \times 10^6/\text{s sr } \mu\text{A}$  for a proton energy of 1980 keV.

For a given angle between the neutron and proton directions, the kinematics of the  $(p,n)$  reaction fixes the neutron energy. Most of our measurements were made with a proton beam of energy 1980 keV and with the neutron target [the Si(Li) detector] placed at 30 deg with respect to the proton beam, yielding a mean neutron energy of 200 keV. Time-of-flight measurements made with a scintillator placed at the same angle indicated a spread in neutron energy (FWHM) of 20 keV under these conditions. The main contribution to this spread comes from the proton energy loss in the  ${}^7\text{Li}$  target before the  $(p,n)$  reaction.

The experimental apparatus (Fig. 1) consisted of two main elements, the Si(Li) target-nuclear recoil spectrometer, and a scintillator counter to detect the scattered neutron.

The Si(Li) was a 4.4-mm-diameter, 3-mm-thick wafer

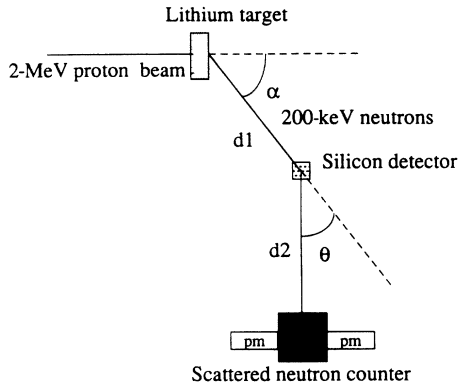


FIG. 1. Top view of the experimental setup. Working conditions correspond to  $\alpha = 30^\circ$ ,  $d_1 = 10$  cm,  $d_2 = 100$  cm,  $\theta$  from  $41^\circ$  to  $107^\circ$ .

mounted on a lightweight aluminium support. The support was connected to a copper cold finger that bathed in a tank of liquid nitrogen. The active element was contained in a 7.5-cm-diameter aluminium vacuum can. The thickness of the aluminium comprising the can was 0.3 mm allowing for good transmission of neutrons and calibrating x rays.

The known energy of  $^{55}\text{Fe}$  x rays (5.9 keV) and  $^{241}\text{Am}$  (13.9, 17.6, and 59.5 keV) were used to establish the energy scale. Since nuclear recoils do not produce the same ionization as an x ray of the same energy, we will refer to the measured energy on the scale established by x rays as the “equivalent electron energy” (EEE).

The charge collected in the Si(Li) detector passed through a low-noise preamplifier mounted on the cryostat, followed by a Tennelec TC 244 shaping amplifier. This signal then went to a fast discriminator for triggering purposes, to a constant fraction discriminator for timing, and to a Lecroy 2259 analog-to-digital (ADC) for the energy measurement. The peaking time of the shaping amplifier was chosen to be  $4 \mu\text{s}$  which allowed sufficient time resolution to determine the accelerator pulse in which a neutron scattering event occurred. The energy resolution as measured with x rays from  $^{55}\text{Fe}$  and  $^{241}\text{Am}$  sources was 410 eV (EEE) (FWHM). The linearity of the system and trigger efficiency were checked with a pulser system. The trigger discriminator efficiency rose from 0 to 100% over a pulse-height interval corresponding to 540 to 610 eV (EEE).

The scintillator used to detect the scattered neutron was a  $(5 \times 8 \times 2)$ -cm<sup>3</sup> block of NE110 viewed by two XP 2020 photomultipliers. The signals from the two photomultipliers were separately discriminated at the level of one photoelectron and then put in coincidence for triggering and timing purposes. The detection efficiency for 200-keV neutrons was 48%. The scintillator viewed the Si(Li) detector through a paraffin collimator so as not to be exposed to neutrons coming directly from the lithium target. The collimator was a 78-cm-long, 60-cm-diameter cylinder with a tapered hole along the axis, 3 cm in diameter near the Si(Li) detector and 10 cm in diameter near the scintillator.

In the nominal operating condition, the Si(Li) detector was positioned 10 cm from the lithium target at an angle of  $30^\circ$  from the proton beam. The scintillator was positioned about 100 cm from the Si(Li) detector. The scattering angle of neutrons could then be varied to select a silicon recoil energy as determined by the  $(p, n)$  and elastic-scattering kinematics. Recoil energies between 3.2 and 21.7 keV were selected.

The trigger was a  $10\text{-}\mu\text{s}$  coincidence between the Si(Li) detector and the scintillator counter. For each event, we recorded the Si(Li) pulse height, the time interval between the scintillator and Si(Li) pulses, and the time interval between the scintillator and the proton beam pulse as determined by an inductive pickup coil.

Figure 2(a) shows a typical distribution of the time between the proton beam pulse and the Si(Li) signal. The  $1\text{-}\mu\text{s}$  period between proton pulses is clearly seen. Most events result from accidental coincidences between a neutron scattered in the silicon and a signal in the scintillator from the same or another beam pulse. The good “in-time” events are expected to be in the central peak.

Figure 2(b) shows the distribution of the time interval between the proton beam pulse and the scintillator signal for the events in the central peak of Fig. 2(a). Three components can be observed: (i) a flat background coming from coincidences between the Si(Li) signal and a hit in the scintillator counter due to the detector noise, multiply scattered neutrons or capture  $\gamma$ , (ii) a first peak due to

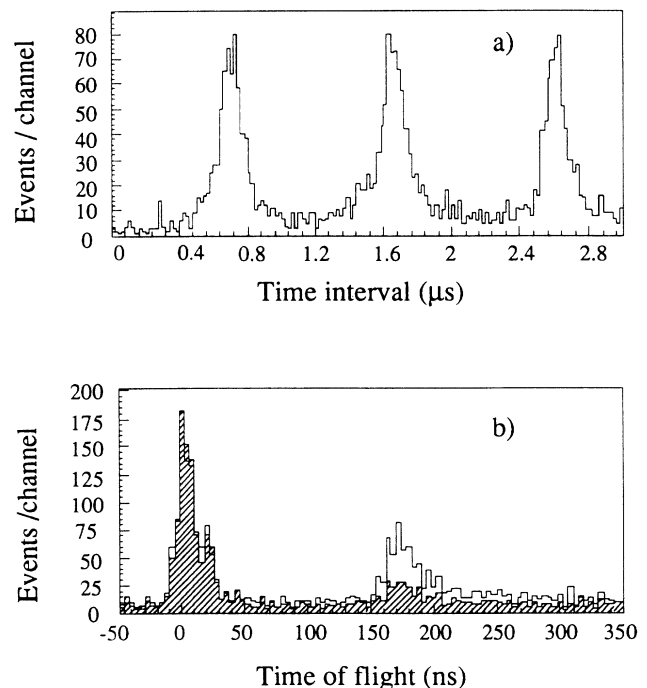


FIG. 2. (a) Typical distribution of time intervals between the Si(Li) signal and the proton beam pulse. The  $1\text{-}\mu\text{s}$  period between beam pulses is clearly seen. Good in-time events are expected in the central peak. (b) Distribution of time intervals between the beam pulse and the scintillator signal for events in the central peak of (a). The expected background due to uncorrelated counts is shaded.

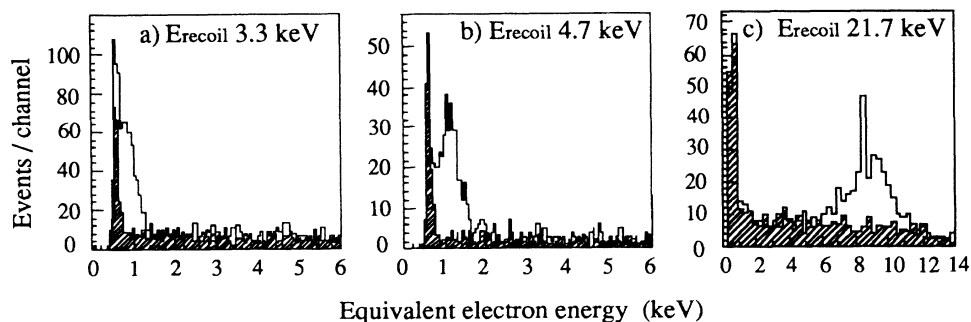


FIG. 3. (a)–(c) Silicon-detector pulse-height distributions for the signal events selected in the central peak of Fig. 2(a) and in the neutron peak of Fig. 2(b) for three recoil energies. The shaded histograms represent the background contribution.

$\gamma$ 's produced in the tantalum target support going directly in the scintillator counter in coincidence with a neutron interacting in the Si(Li) detector, and (iii) a second delayed peak due to neutrons that have scattered on the Si(Li) detector or its aluminium support and reached the scintillator counter.

The shape and amplitude of the background have been obtained from the two “out-of-time” beam pulses of Fig. 2(a); it is shown on the shaded histogram of Fig. 2(b). The signal due to neutrons scattered off silicon nuclei and detected in the scintillator counter appears now clearly above the background, at a time relative to the first  $\gamma$  peak which does correspond to the expected time of flight. The background distribution does also exhibit a small bump at the same timing. It comes from accidental coincidences between hits in the scintillation counter due to neutrons scattered off passive materials around silicon diode, mainly aluminium (with the same timing, as aluminium and silicon have approximately the same mass), and uncorrelated hits in the silicon diode. This illustrates the efficiency of the background rejection achieved with a pulsed beam.

Figures 3(a)–3(c) show the distribution of Si(Li) pulse height (in keV, EEE) for the events selected in the central

peak of Fig. 2(a) and in the neutron peak of Fig. 2(b). The different histograms correspond to three different recoil energies as determined by the scattering angle and neutron energy. The shaded parts represent the accidental-coincidence background contribution. Their shape and amplitude were estimated with the events from the “out-of-time” beam pulses of Fig. 2(a) with the same time of flight selection as for the signal on Fig. 2(b). The almost flat component of the background under the signal peaks is due to neutrons scattered off the silicon nuclei at all angles. For the incident neutron energy considered here, this distribution is indeed expected to be flat up to the maximum recoil energy as a consequence of the isotropic angular distribution in the center of mass. The sharp rise at low energy is due to the electronic noise of the Si(Li) detector and puts a limit to the lowest recoil energy which can be reliably measured at around 3 keV.

After background subtraction, the signal peaks were fitted with a Gaussian to determine the mean and the width of the observed energy distribution. Table I gives, for each recoil energy, the mean observed energy (EEE) and the ratio between the mean observed energy and the calculated recoil energy. The uncertainty in the calculated recoil energy is due to the experimental geometry and

TABLE I. Summary of the results. For each calculated silicon energy are given, the mean observed ionization energy [so-called equivalent electron energy (EEE), that is the electron energy which would give the same signal as the one observed from the silicon recoil], the ionization efficiency (ratio between columns 2 and 1), the width of the observed signal distribution, the expected instrumental width, and the noninstrumental width relative to the calculated one. Quoted errors and widths correspond to  $1\sigma$  (rms).

Silicon recoil energy (keV)	Ionization (keV) (EEE)	Efficiency (%)	Peak width (eV) (EEE)	Calculated contribution to width (eV) (EEE)	Calculated noninstrumental width (eV) (EEE)
$3.3 \pm 0.1$	$0.85 \pm 0.05$	$25.9 \pm 1.6$	$227 \pm 32$	$186 \pm 5$	$131 \pm 55$
$3.9 \pm 0.1$	$0.89 \pm 0.08$	$22.9 \pm 2.0$	$304 \pm 52$	$185 \pm 5$	$241 \pm 66$
$4.15 \pm 0.1$	$1.14 \pm 0.02$	$27.4 \pm 0.8$	$253 \pm 25$	$190 \pm 5$	$166 \pm 39$
$4.7 \pm 0.1$	$1.25 \pm 0.03$	$26.6 \pm 0.8$	$266 \pm 25$	$191 \pm 5$	$185 \pm 36$
$8.6 \pm 0.1$	$2.66 \pm 0.02$	$31.1 \pm 0.5$	$411 \pm 11$	$218 \pm 6$	$348 \pm 13$
$13.5 \pm 0.3$	$4.53 \pm 0.06$	$33.6 \pm 0.7$	$680 \pm 37$	$317 \pm 11$	$601 \pm 42$
$19.5 \pm 0.2$	$7.56 \pm 0.11$	$38.7 \pm 0.7$	$1155 \pm 103$	$348 \pm 9$	$1101 \pm 108$
$21.7 \pm 0.2$	$8.79 \pm 0.08$	$40.7 \pm 0.5$	$1058 \pm 56$	$346 \pm 13$	$1000 \pm 59$

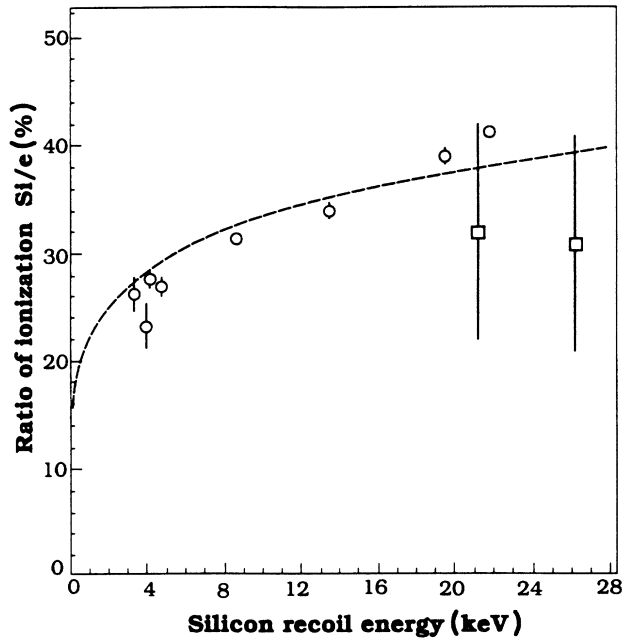


FIG. 4. Ratio between the observed energy [equivalent electron energy (EEE)] and the calculated recoil energy as a function of the silicon recoil energy. Circles are data points from the present experiment, squares are data points from Sattler's experiment (Ref. 8). The curve represents the result of the calculation of Lindhard *et al.* (Ref. 6).

beam energy. The uncertainty in the determination of the mean observed energy (EEE) is primarily statistical, with a small contribution due to the uncertainty in the energy scale.

Figure 4 shows the ratio between the observed energy and the calculated recoil energy as a function of the recoil energy for the eight energies measured in this ex-

periment. Also shown are the two lowest-energy points obtained by Sattler.<sup>8</sup> The superimposed curve is taken from the Lindhard *et al.* calculation in the case of silicon (cf. Ref. 6, p. 26, Fig. 3 for the value of their parameter  $k$  equal to 0.15). There is reasonable agreement between the observed and theoretical values, especially considering that Lindhard *et al.* state that the assumptions made in their model may lead to errors of order 5% to 10%.

The fourth and fifth entries in Table I give the width (1  $\sigma$ , rms) of the observed energy distribution and the calculated instrumental contribution to the width. Contributions to the expected width are, by order of importance, the electronic noise, the spread of the Si recoils due to the sizable solid angle of the scintillator viewed by the Si(Li) detector, and the spread of neutron energies. The sixth entry shows the noninstrumental width and error. This excess width becomes significant at high recoil energies and indicates the presence of fluctuations in the ionization process for nuclear recoils that are not present in the case of photoelectrons. Such fluctuations were predicted by Lindhard *et al.* but calculated reliably only at higher energies.

In summary, we have observed recoils of silicon nuclei of energies in the range 3.2–21 keV in a Si(Li) detector. The ratios between the ionization produced by a recoil silicon nucleus and an electron ranges from 0.25 at 3.3 keV up to 0.40 at 21 keV. These data serve to calibrate a Si(Li) dark-matter detector whose results are discussed in Ref. 5.

We would like to thank J. Poinignon and J. P. Soirat for their support in preparing the experimental setup and M. Morel and M. Mariani for operating the accelerator. This work was supported in part by the Institut de Recherche Fondamentale, Commissariat à l'Energie Atomique, France, and in part by the U.S. Department of Energy and the National Science Foundation.

<sup>1</sup>M. W. Goodman and E. Witten, *Phys. Rev. D* **31**, 3059 (1985).

<sup>2</sup>S. P. Ahlen *et al.*, *Phys. Lett. B* **195**, 603 (1987); D. O. Caldwell *et al.*, *Phys. Rev. Lett.* **61**, 520 (1988).

<sup>3</sup>B. Sadoulet, J. Rich, M. Spiro, and D. O. Caldwell, *Astrophys. J.* **324**, L75 (1988); J. Rich, R. Rochia, and M. Spiro, *Phys. Lett. B* **194**, 173 (1987).

<sup>4</sup>J. Faulkner and R. L. Gilliland, *Astrophys. J.* **299**, 994 (1985); D. N. Spergel and W. H. Press, *ibid.* **294**, 663 (1985); W. H. Press and D. N. Spergel, *ibid.* **296**, 679 (1985); R. Gilliland *et al.*, *ibid.* **306**, 679 (1985).

<sup>5</sup>D. O. Caldwell *et al.*, *Phys. Rev. Lett.* **65**, 1305 (1990); in *Theoretical and Phenomenological Aspects of Underground Physics*, proceedings of the Workshop, L'Aquila, Italy, 1989, edited by A. Bottino and P. Monacelli (Editions Frontières, Gif-sur-Yvette, France, 1989).

<sup>6</sup>J. Lindhard, V. Nielsen, M. Scharff, and P. V. Thomsen, *Mat. Fys. Medd. Dan. Vid. Selsk.* **33**, 10 (1963).

<sup>7</sup>C. Chasman, K. W. Jones, and R. A. Ristinen, *Phys. Rev. Lett.* **15**, 245 (1965).

<sup>8</sup>A. R. Sattler, *Phys. Rev.* **138**, A1815 (1965).

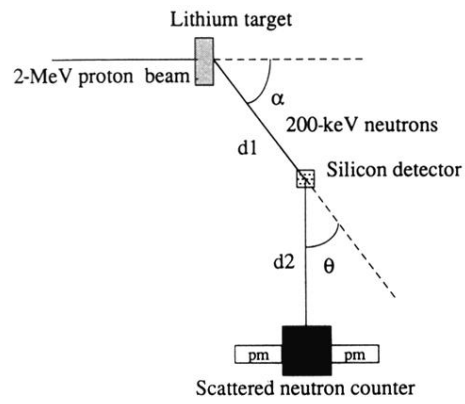


FIG. 1. Top view of the experimental setup. Working conditions correspond to  $\alpha = 30^\circ$ ,  $d_1 = 10$  cm,  $d_2 = 100$  cm,  $\theta$  from  $41^\circ$  to  $107^\circ$ .